Nano Res
DOI 10.1007/s12274-012-0273-7
Research Article

ISSN 1998-0124
CN 11-5974/O4

Fabrication of Patterned Boron Carbide Nanowires and Their Electrical, Field Emission, and Flexibility Properties

Yuan Huang[1], Fei Liu[2], Qiang Luo[1], Yuan Tian[1], Qiang Zou[1], Chen Li[1], Chengmin Shen[1], Shaozhi Deng[2], Changzhi Gu[1], Ningsheng Xu[2], and Hongjun Gao[1] (✉)

[1] Beijing National Laboratory for Condensed Matter Physics, Institute of Physics, Chinese Academy of Sciences, Beijing 100190, China
[2] State Key Laboratory of Optoelectronic Materials and Technologies, Guangdong Province Key Laboratory of Display Material and Technology, and School of Physics and Engineering, Sun Yat-sen University, Guangzhou 510275, China

Received: 16 August 2012 / Revised: 9 October 2012 / Accepted: 15 October 2012

ABSTRACT

Large-area patterned boron carbide nanowires (B_4C NWs) have been synthesized using chemical vapor deposition (CVD). The average diameter of B_4C NWs is about 50 nm, with a mean length of 20 μm. The B_4C NWs have a single-crystal structure and conductivities around $5.1 \times 10^{-2}\ \Omega^{-1}\cdot cm^{-1}$. Field emission measurements of patterned B_4C NWs films show that their turn-on electric field is 2.7 V/μm, lower than that of continuous B_4C NWs films. A single nanowire also exhibits excellent flexibility under high-strain bending cycles without deformation or failure. All together, this suggests that B_4C NWs are a promising candidate for flexible cold cathode materials.

KEYWORDS

Boron carbide nanowires, patterned, field emission properties, flexible

1. Introduction

Boron carbide (B_4C) is an important non-metallic material because of its unique structure and exceptional physicochemical properties: high melting point, low density, extreme hardness, high strength, high Young's modulus and large Seebeck coefficient [1–4]. Because of these features, B_4C exhibits excellent mechanical and thermoelectric properties. Therefore, B_4C materials have a great many applications in high-temperature thermoelectric energy conversion and field emission (FE) flat-panel displays. On the other hand, B_4C also has the ability to capture neutrons [3], and can therefore be used as a neutron absorber in the nuclear industry [5]. Previous studies have indicated that B_4C one-dimensional (1D) nanostructures exhibit some novel properties differing from their bulk materials [6, 7].

In the past decade, boron carbide 1D nanostructures have attracted much attention [8]. B_4C nanomaterials with different morphologies such as nanowires [9], nanobelts [10] and nanosprings [11] have been prepared using diverse methods. These B_4C nanostructures exhibit special electrical, optical, and mechanical properties [6, 9, 12]. Tao et al. reported that B_4C nanowire/carbon-microfiber hybrid structures have a high elastic modulus of 428.1 GPa ± 9.3 GPa and can block 99.8% UV radiation [6]. Tian et al. investigated field emission properties of B_4C NWs and indicated that B_4C NWs are a potential candidate for nanoscale cold cathode materials [12]. Despite these advances,

Address correspondence to hjgao@ iphy.ac.cn

there have been few investigations of the electrical, mechanical and field emission properties of B_4C 1D nanostructures. In particular, the preparation of patterned B_4C 1D nanostructures has yet to be reported. The growth of aligned 1D nanostructure arrays is a crucial factor for FE flat-panel displays because it can reduce screen effects among 1D nanostructures and improve their field emission properties. As such, this calls for a simple method to prepare well-controlled, high-yield, and pure 1D boron carbide nanostructures.

In the research described in this paper, we used a comparatively simple method to make a pattern of Fe_3O_4 catalyst nanoparticles on Si (111) substrate, using a Mo grid template as a mask [13]. High density and large-area B_4C NW patterns were synthesized on the substrate. High-resolution transmission electron microscopy (HRTEM) and electron energy loss spectroscopy (EELS) analysis indicate that B_4C NW has a single-crystal structure. The field emission properties of patterned B_4C NWs and continuous B_4C NWs were compared. The physical properties of individual B_4C NW were also investigated in order to test their potential for applications in flexible cathode nanomaterials.

2. Experimental

2.1 Materials

Boron powder (99.99%), B_2O_3 (99.99%), carbon powder (99.9%), and iron powder (99.99%) with a weight ratio of 2:1:1:1 were used as source materials. Hydrophilic Fe_3O_4 nanoparticles, to serve as catalysts, with an average diameter of 20 nm, were prepared by a straightforward alkaline deposition method we have reported before [14].

2.2 Preparation of patterned B_4C nanowires

The patterned B_4C NWs were fabricated following a simple method, using a special Mo mask as a template [13]. The process for the synthesis of patterned nanowires comprises four steps illustrated in Fig. 1. In the first step, a square Mo grid mask with a length of 25 mm was fixed on the surface of the Si (111) substrate. Then, the Fe_3O_4 catalyst solution mixed with boron powder was dropped onto the Mo mask coating Si (111) substrate. The Mo mask was removed from Si (111) substrate leaving a pattern of catalyst nanoparticles after the solution was evaporated completely. Finally, large-area patterned B_4C NWs were prepared by CVD.

A horizontal tube furnace with an accurate controller of both the temperature and the gas flow rate was used for growth of the B_4C NWs. Boron powder, B_2O_3, C and Fe powder with a mass ratio of 2:1:1:1 were milled together as reaction precursors and loaded into a ceramic boat. The Si (111) substrate catalyst coating pattern was placed behind the precursors, after which the furnace temperature was raised to 400 ℃ in 15 min and maintained for 30 min under an argon flow (300 (standard cubic centimeters per minute (sccm)) to remove organic ligands capped on the surface of catalyst nanoparticles. Then the temperature of the reaction region was increased to 1100 ℃ in 1 h, and the flow rate of argon gas was adjusted to 50 sccm. The reaction was allowed to continue for 2 hours at this temperature. Finally, the tube furnace was cooled down to room temperature, and it was observed that patterned B_4C NWs had been obtained on the Si (111) substrate.

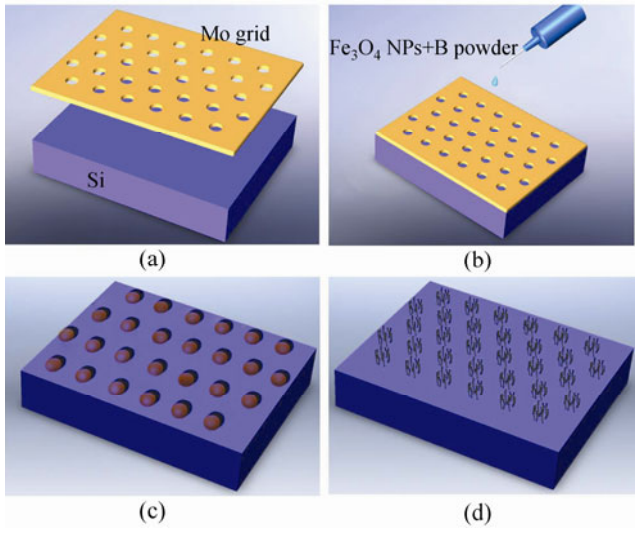

Figure 1 The fabrication process of patterned B_4C NWs: (a) schematic image of a Mo grid flake and Si (111) substrate; (b) and (c) dropping and drying the catalyst solution on the Si (111) using Mo grid as mask; (d) patterned nanowires grown by chemical vapor deposition

2.3 Characterization of B_4C NWs

The morphology and crystalline structure of the nanowires were characterized by field emission scanning electron microscopy (FE-SEM: SFEG, FEI Corp), transmission electron microscopy (TEM: Tecnai-20, Philips Corp.) and HRTEM (Tecnai F20, FEI Corp.). Electron energy loss spectroscopy was employed to obtain the chemical composition. Measurements of the FE properties of patterned B_4C NWs were performed on a high vacuum FE analysis system. The flexibility properties of individual B_4C NW were observed in a focused ion beam etching and depositing system (FIB: DB235, FEI Corp.).

3. Result and discussion

Large area patterned B_4C NWs were grown on the surface of the Si (111) substrate using a Mo mask as template (Fig. 2). Figure 2(a) shows the SEM image of a large area of the patterned B_4C NWs. It can be clearly seen that high density and large area patterned B_4C NWs with uniform cell size were obtained. From a high magnification SEM image (Fig. 2(b)), the diameter of the patterned unit is found to be about 100 μm and the distance between two neighboring patterned units is 80 μm, close to the size of the Mo mask. No B_4C NWs can be observed in the bottom of channels between two patterned units. Figures 2(c) and 2(d) show B_4C NWs standing vertically on the Si (111) substrate. This orientation will improve their field emission properties. The as-prepared B_4C NWs have an average diameter of 50 nm and length of 20 μm. The bright particles on the tips of nanowires should be the Fe_3O_4 catalyst, which implies that the growth mechanism may follow a vapor–liquid–solid (VLS) process.

Details of the crystalline structure of B_4C NWs were obtained by TEM and HRTEM. Figure 3(a) shows a low magnification TEM image of individual B_4C NWs. It can be seen that the surface of the nanowire is very smooth and its diameter is about 50 nm. The selected area electron diffraction (SAED) pattern of the nanowire was measured in the middle of the B_4C NW (lower left corner in Fig. 3(a)). Clear diffraction spots are obviously seen in the SAED pattern, which suggests that B_4C NW has a single-crystal structure. From the HRTEM image (top right corner in Fig. 3(a)), it can be seen that the B_4C NW has perfect crystalline lattice fringes without observable defects. The B_4C NW grew along the [101] direction, in accordance with earlier reports [10, 15]. The chemical composition of this nanowire was analyzed by EELS. Figure 3(b) shows a typical EELS spectrum obtained from a single nanowire. Ionization edges around 190 and 284 eV are observed in the spectrum, which respectively correspond to the

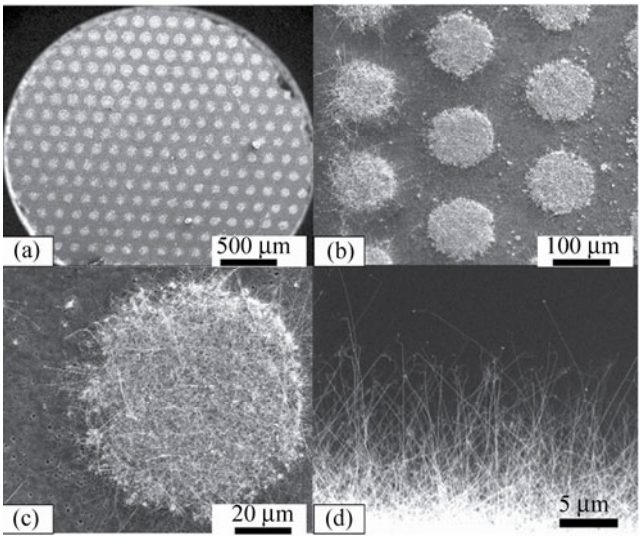

Figure 2 SEM image of B_4C NWs: (a), (b) and (c) are the top views of patterned B_4C NWs; (d) a typical side view of B_4C NWs

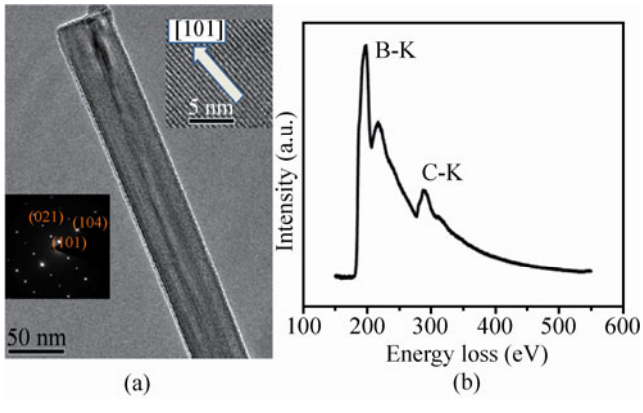

Figure 3 Structural and component analysis of B_4C NW. (a) TEM image of a single boron carbide nanowire; the top right-hand corner inset shows the HRTEM image of the boron carbide nanowires, the growth orientation is along [101]; the lower left-hand corner inset shows the SAED pattern of the B_4C NW. (b) Typical EELS spectrum of the nanowire

K-edges of B and C. The atomic ratio of B to C is about 4.06, which is consistent with the stoichiometry of B_4C. No oxygen, iron or other elements can be detected in the spectrum, which indicates B_4C NWs are pure single crystals.

The electrical properties of bulk B_4C materials have been explored by other research groups [1, 16]. However, the electrical transport properties of a one-dimensional nanostructure such as these patterned B_4C NWs have not been reported in detail, although this is crucial for their future applications. The measurements were carried out in a modified high-vacuum SEM system. Two individual B_4C NWs on the Si (111) substrate were chosen for the measurements. The electrical transport properties of a single B_4C NW are given in Figs. 4(a) and 4(b) and the insets of Figs. 4(a) and 4(b) respectively give the SEM images of the measurement process of two B_4C NWs. In Fig. 4(a), the *I*–*V* curves of the nanowire were found to be divided into two sections, which can be illustrated by the thermal electron field emission model [17]. We conclude that the total resistance R_t mainly consists of two parts, namely, the intrinsic resistance R_i of the B_4C NW and the contact resistance R_c. At low voltages, the current is almost without change. After the voltage exceeds a transitional voltage $V_{critical}$ (about 6 V in this experiment), the current increases dramatically. According to the thermal electron field-emission model [17], the intrinsic resistance of these two nanowires can be derived from the slope of the of the *I*–*V* curves

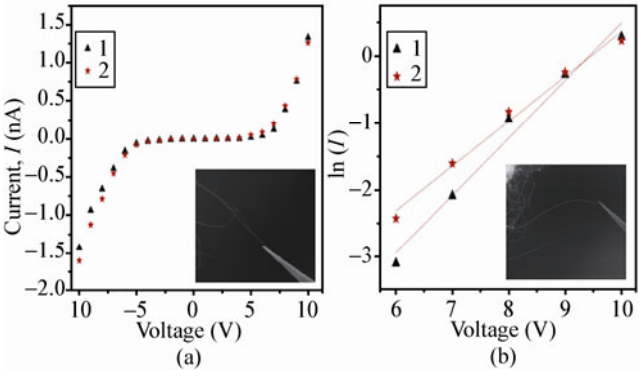

Figure 4 Electrical transport measurements of B_4C NWs: (a) the *I*–*V* curves of two individual B_4C NWs during conductivity measurement under room temperature; (b) the corresponding ln *I*–*V* curves of these two nanowires. The SEM images of the two nanowires contacted by a W probe are given in the insets (a) and (b)

in the high voltage ($V > V_{critical}$) region, and the $V_{critical}$ is related to the Schottky barrier. In the low voltage region, the total resistance is dominated by contact resistance. The intrinsic resistance of a B_4C NW R_i may be expressed as

$$R_i = \rho \frac{l}{s} = \frac{l}{\sigma s}$$

So we can easily write

$$\sigma = \frac{l}{R_i S} \quad (1)$$

where ρ is the intrinsic resistivity and σ is the conductivity of B_4C NW, and l and s are the length and cross area of individual nanowire. The conductivities of the two nanowires were calculated to be 5.85×10^{-2} and 4.36×10^{-2} $\Omega^{-1}\cdot cm^{-1}$, thus the average conductivity is about 5.1×10^{-2} $\Omega^{-1}\cdot cm^{-1}$, which is higher than the conductivity of boron NWs [18] and close to that of a BN nanotube [19]. Based on thermionic-field emission theory, the relationship between ln*I* and *V* ($V > V_{critical}$) can be written as

$$\ln I = \left(\frac{q}{KT} - \frac{1}{E}\right) \times V + \ln I_{sr} \quad (2)$$

where *I* is the total current in the high-voltage regime, *E* is the field at the cathode–vacuum interface, and I_{sr} is the current under the Schottky barrier at reverse bias voltage. According to Eq. (2), the plot of ln*I* vs. *V* should be linear, which fits well with our experimental results in Fig. 4(b); further details can be seen in the Electronic Supplementary Material (ESM).

In the past few years, our group have reported FE properties of boron NWs [18, 20, 21] and boron nanocones [13, 22]. These results collectively showed that one-dimensional boron nanostructures are a candidate nanoscale cold cathode material [20]. Although bulk B_4C materials have both physical and chemical properties similar to those of bulk boron materials, reports on the FE properties of B_4C nanostructure are few. Tian et al. [12] reported a two-step field emission of high density B_4C NWs film, which derived from physical breakage in the B_4C NWs.

We compared the FE properties of our patterned B_4C NWs and continuous B_4C NW films to determine their field emission properties. Figure 5 shows typical

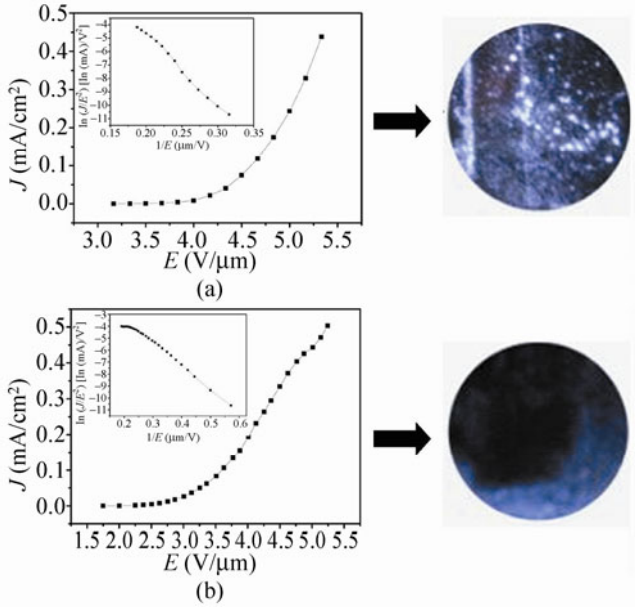

Figure 5 FE properties of B_4C NWs. (a) and (b) are the *J*–*E* curves and corresponding FN plots of patterned and continuous B_4C NWs, respectively. The spatial distribution of emission sites on the substrate are shown at the right side of (a) and (b), and the bright spots correspond to the electron emission sites

curves of their emission current density versus electrical field (*J*–*E*). The turn-on field (defined as the electric field for $J = 10$ μA/cm^2) of the randomly grown B_4C NWs is 4.1 V/μm. For our patterned B_4C NWs, the turn-on field decreased to 2.7 V/μm, which indicates that the patterned growth efficiently improves their field emission properties. Their promising field emission performance arises from the decreased screening effect and quasi-aligned distributions of the nanowires (see Figs. S-1 and S-2 in the ESM). Moreover, the field emission pro- perties of our B_4C NW patterns are better than those of boron films of either nanowires or nanocones [20, 21], and very close to those of ZnO nanoneedle arrays (2.4 V/μm) [23]. The size of the sample was 2 cm × 2 cm, and a transparent anode was used to measure its field emission properties. It can be seen in Fig. 5(a) that most of the groups of nanowires are involved in the emission process, which suggests that B_4C NWs have good emission uniformity.

The Fowler–Nordheim (FN) equation can be used to illustrate their FE mechanism [24]. The current density can be written as

$$J = A\left(\frac{\beta^2 E^2}{\Phi}\right)\cdot\exp\left(\frac{-\beta\Phi^{\frac{3}{2}}}{\beta E}\right) \tag{3a}$$

So, the FN plots are generally derived as:

$$\ln\left(\frac{J}{E^2}\right) = -\frac{B\Phi^{\frac{3}{2}}}{\beta}\frac{1}{E} + \ln\left(\frac{\beta^2}{A\Phi}\right) \tag{3b}$$

where E is the applied electric field, and Φ is the work function of the sample, which for boron NWs is 4 eV. In this equation, $A = 1.57 \times 10^{-10}$ A·V^2·eV, $B = 6.83 \times 10^9$ V·m^{-1}·eV$^{-3/2}$. The field enhancement factors β for the patterned and un-patterned samples were calculated to be 3070 and 1000, respectively. The field enhancement factor of the patterned substrate is three times that of the continuous film, which suggests that patterned growth raises the enhancement factor significantly. In addition, this high enhancement factor is helpful for their future FE applications.

It is well known that boron carbide is hard and brittle in nature [25]. But recent studies in our group reveal that boron NWs have excellent flexibility [26]. In the present study we also investigated the flexibility of a single B_4C NW in a focused ion beam etching and depositing system (FIB). A B_4C NW tip was prepared on the Au-probe in advance. The detailed fabrication procedure is as follows. First, the gold probe was gradually moved into contact with an individual B_4C NW, and a DC voltage was applied between the B_4C NW and the Au probe. This process may be dominated by a thermal effect. After gradually applying a DC voltage, the current will induce a dramatic increase in temperature seen at 23 V. At the critical temperature, the nanowire will fragment, leaving a part of the nanowire welded onto the probe (Figs. 6(a) and 6(b)). From high-resolution SEM images (Fig. 6(d)), we can clearly see that the B_4C NW tip may be formed in a "U" shape. This indicates that a nanoscale tip is easily prepared by this method.

The B_4C NW tip on the Au-probe was placed in contact with a single straight B_4C NW. After that, we manipulated this B_4C NW tip on the Au-probe to gradually press another individual B_4C NW. The stressing process of the nanowire is shown in Figs. 7(a)–7(d) and the corresponding releasing process is given

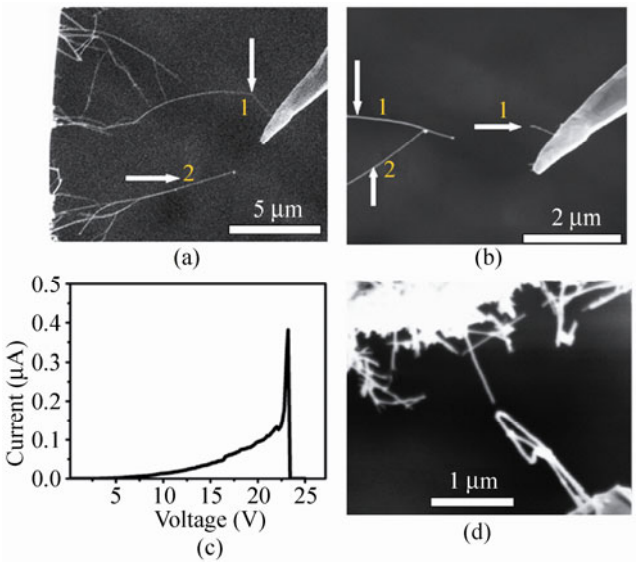

Figure 6 (a) Image of the gold-probe contact with an individual nanowire. (b) SEM image of broken nanowire welded on the side of gold probe during high voltage. (c) Corresponding measured *I*–*V* curve of the nanowire (1). (d) SEM image of the gold probe with attached nanowire bent in a needle's eye-like structure

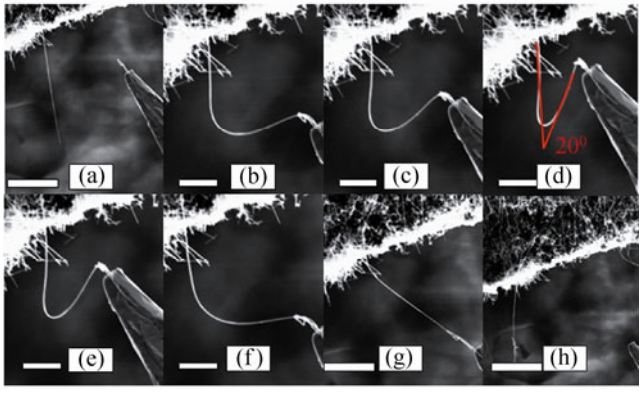

Figure 7 SEM images of the bending process: (a)–(d) the stressing process, and (e)–(h) the release process recorded by SEM images. After the release process, the NW once on the tip of the Au-probe was hung over the tested NW. The scale bar for images (b)–(f) is 2 μm, and for (a), (g) and (h) is 5 μm

in Figs. 7(e)–7(h). The B_4C NW was bent to a sharp angle of 20° without any fracture, and the deformation ratio was nearly 89%. It is proposed that the mechanical properties of B_4C NW are better than other one-dimensional nanomaterials, such as B NWs and ZnO NWs. The flexibility of B_4C NWs obviously surpasses that of bulk boron carbide. This can be accounted for by the many defects that exist in bulk boron carbide materials, possibly limiting flexibility and making the boron carbide brittle under high stress. However, B_4C NWs are perfect single crystals without defects. One can also point to the fact that B_4C NWs have a higher aspect ratio, which ensures that they can sustain larger deformation.

Tao, et al. conducted similar experiments in a TEM instrument [6], one difference being that the nanowire used in our experiment was straight, while Tao used a bent nanowire. They used an STM probe to manipulate an individual B_4C NW, which is more difficult to control. Thus, compared with their experiment, our method is simpler and easily accomplished. The deformation ratio in their experiment was about 45%, which is about half the ratio found in our experiment. These results indicate that B_4C NW is an excellent flexible material.

4. Conclusions

High density and patterned B_4C NWs have been fabricated by chemical vapor deposition. These nanowires have mean lengths of 20 μm and diameters of 50 nm. HRTEM and EELS results show that they are good crystals. The average conductivity is about $5.1 \times 10^{-2} \cdot \Omega^{-1} \cdot cm^{-1}$. The field emission properties were enhanced by the patterning technique of fabrication. Moreover, the nanowires exhibit more excellent flexibility than bulk boron carbide material and can survive deformation of nearly 160°. This ultimately suggests that boron carbide nanowires are promising candidates for electronic applications requiring a flexible material.

Acknowledgements

The work was supported by the National Natural Science Foundation of China (Grant Nos. 50872147, 51072237, U0734003, 50802117, 51072237 and 50725206), the Foundation of Education Ministry of China (2009-30000-3161452), the National Basic Research Program of China (973 Program, Grant No. 2013CB933604) and China Scholarship Council Fund for Young Backbone Teachers.

Electronic Supplementary Material: Supplementary material (details of the electrical and field emission properties measurement) is available in the online version of this article at http://dx.doi.org/10.1007/s12274-012-0273-7.

References

[1] Wood, C.; Emin, D. Conduction mechanism in boron carbide. *Phys. Rev. B* **1984**, *29*, 4582–4587.

[2] Zhou, M. J.; Wong, S. F.; Ong, C. W.; Li, Q. Microstructure and mechanical properties of B_4C films deposited by ion beam sputtering. *Thin Solid Films* **2007**, *516*, 336–339.

[3] Knotek, O.; Lugscheider, E.; Siry, C. W. Tribological properties of B–C thin films deposited by magnetron-sputter-ion plating method. *Surf. Coat. Technol.* **1997**, *91*, 167–173.

[4] Aselage, T. L.; Emin, D.; McCready, S. S.; Duncan, R. V. Large enhancement of boron carbides' Seebeck coeffiecients through vibrational softening. *Phys. Rev. Lett.* **1998**, *81*, 2316–2319.

[5] Caruso, A. N.; Dowben, P. A.; Balkir, S.; Schemm, N.; Osberg, K.; Fairchild, R. W.; Flores, O. B.; Balaz, S.; Harken, A. D.; Robertson, B. W.; Brand, J. I. The all boron carbide diode neutron detector: Comparison with theory. *Mater. Sci. Eng. B* **2006**, *135*, 129–133.

[6] Tao, X. Y.; Dong, L. X; Wang, X. N.; Zhang, W. K.; Nelson, B. J.; Li, X. D. B_4C-nanowires/carbon-microfiber hybrid structures and composites from cotton T-shirts. *Adv. Mater.* **2010**, *22*, 2055–2059.

[7] Tian, J. F.; Xu, Z. C.; Shen, C. M.; Liu, F.; Xu, N. S.; Gao, H. J. One-dimensional boron nanostructures: Prediction, synthesis, characterizations, and applications. *Nanoscale* **2010**, *2*, 1375–1389.

[8] Mondal, S.; Banthia, A. K. Low-temperature synthetic route for boron carbide. *J. Eur. Ceram. Soc.* **2005**, *25*, 287–291.

[9] Bao, L. H.; Li, C.; Tian, Y.; Tian, J. F.; Hui, C.; Wang, X. J.; Shen, C. M.; Gao, H. J. Synthesis and photoluminescence property of boron carbide nanowires. *Chin. Phys. B* **2008**, *17*, 4585–4591.

[10] Bao, L. H.; Li, C.; Tian, Y.; Tian, J. F.; Hui, C.; Wang, X. J.; Shen, C. M.; Gao, H. J. Single crystalline boron carbide nanobelts: Synthesis and characterization. *Chin. Phys. B* **2008**, *17*, 4247–4252.

[11] McIlroy, D. N.; Zhang, D.; Kranov, Y.; Norton, M. G. Nanosprings. *Appl. Phys. Lett.* **2001**, *79* 1540–1542.

[12] Tian, J. F.; Bao, L. H.; Wang, X. J.; Hui, C.; Liu, F.; Li, C.; Shen, C. M.; Wang, Z. L.; Gu, C. Z.; Gao, H. J. Probing field emission from boron carbide nanowires. *Chin. Phys. Lett.* **2008**, *25*, 3463–3466.

[13] Li, C.; Tian, Y.; Hui, C.; Tian, J. F.; Bao, L. H.; Shen C. M.; Gao, H. J. Field emission properties of patterned boron nanocones. *Nanotechnology* **2010**, *21*, 325705.

[14] Hui, C.; Shen, C. M.; Yang, T. Z.; Bao, L. H.; Tian, J. F.; Ding, H.; Li, C.; Gao, H. J. Large-scale Fe_3O_4 nanoparticles soluble in water synthesized by a facile method. *J. Phys. Chem. C* **2008**, *112*, 11336–11339.

[15] Ma, R. Z.; Bando, Y. Investigation on growth of boron carbide nanowires. *Chem. Mater.* **2002**, *14*, 4403–4407.

[16] Schmechel, R.; Werheit, H. Structural defects of some icosahedral boron-rich solids and their correlation with the electronic properties. *J. Solid State Chem.* **2000**, *154*, 61–67.

[17] Zhang, Z. Y.; Yao, K.; Liu, Y.; Jin, C. H.; Liang, X. L.; Chen, Q.; Peng, L. M. Quantitative analysis of current–voltage characteristics of semiconducting nanowires: Decoupling of contact effects. *Adv. Funct. Mater.* **2007**, *17*, 2478–2489.

[18] Liu, F.; Su, Z. J.; Li, L.; Mo, F. Y.; Jin, S. Y.; Deng, S. Z.; Chen, J.; Shen, C. M.; Gao, H. J.; Xu, N. S. Effect of contact mode on the electrical transport and field-emission performance of individual boron nanowires. *Adv. Funct. Mater.* **2010**, *20*, 1994–2003.

[19] Tang, C. C.; Bando, Y.; Huang, Y.; Yue, S. L.; Gu, C. Z.; Xu, F. F.; Golberg, D. Fluorination and electrical conductivity of BN nanotubes. *J. Am. Chem. Soc.* **2005**, *127*, 6552–6553.

[20] Tian, J. F.; Hui, C.; Bao, L. H.; Li, C.; Tian, Y.; Ding, H.; Shen, C. M.; Gao, H. J. Patterned boron nanowires and field emission properties. *Appl. Phys. Lett.* **2009**, *94*, 083101.

[21] Tian, Y.; Shen, C. M.; Li, C.; Shi, X. Z.; Huang, Y.; Gao, H. J. Synthesis of monodisperse $CoPt_3$ nanocrystals and their catalytic behavior for growth of boron nanowires. *Nano Res.* **2011**, *4*, 780–787.

[22] Wang, X. J.; Tian, J. F.; Yang, T. Z.; Bao, L. H.; Hui, C.; Liu, F.; Shen, C. M.; Gu, C. Z.; Xu, N. S.; Gao, H. J. Single crystalline boron nanocones: Electric transport and field emission properties. *Adv. Mater.* **2007**, *19*, 4480–4485.

[23] Zhu,Y. W.; Zhang, H. Z.; Sun, X. C.; Feng, S. Q.; Xu, J.; Zhao, Q.; Xiang, B.; Wang, R. M.; Yu, D. P. Efficient field emission from ZnO nanoneedle arrays. *Appl. Phys. Lett.* **2003**, *83*, 144–146.

[24] Fowler, R. H.; F. R. S.; Nordheim, L. Electron emission in intense electric fields. *Proc. R. Soc. London, Ser. A* **1928**, *119*, 173–181.

[25] Chen, M. W.; McCauley, J. W.; Hemker, K. J. Shock-induced localized amorphization in boron carbide. *Science* **2003**, *299*, 1563–1566.

[26] Tian, J. F.; Cai, J. M.; Hui, C.; Zhang, C. D.; Bao, L. H.; Gao, M.; Shen, C. M.; Gao, H. J. Boron nanowires for flexible electronics. *Appl. Phys. Lett.* **2008**, *93*, 122105.